

Supporting Information for: "Sweep voltammetry with a semi-circular potential waveform: Electrode kinetics"

Yuki Uchida, Enno Kätelhön, and Richard G. Compton

Department of Chemistry, Physical and Theoretical Chemistry Laboratory, Oxford University, South Parks Road, Oxford, OX1 3QZ, United Kingdom

The following sections contain the convergence test results and additional voltammograms as mentioned in the paper.

S1 Convergence tests

We perform convergence tests for the parameters $\sigma = 3.89$ and $K_0 = 10^2$. As shown in Figure 2 in the main text, this set of parameters lies at the transition from the quasi-reversible to the reversible regime and the peak flux converges to a finite value. Large $K_0 \rightarrow \infty$ approach the reversible limit and alongside an infinite peak flux¹ which cannot be convergently modelled by means of finite differences.

The numerical parameters we consider for the following convergence tests are $\Delta\theta$, h , and ω , and their physical significance is explained along with the corresponding convergence test results. The values used for the figures and analysis reported in the paper are $\Delta\theta = 10^{-4}$, $h = 10^{-6}$, and $\omega = 1.1$, and the justification for using these values are provided below.

The parameter we consider first and which has the greatest influence on the peak current is $\Delta\theta$. $\Delta\theta$ is the discretized potential which indicates how much the potential changes between each time step when a triangular potential wave is employed. Time is also discretized and $\Delta\theta$ is used to calculate the difference between each time step, defined as $\Delta\tau = \frac{\Delta\theta}{\sigma_{avg}}$. The discretized semi-circular potential wave equation is:

$$\theta(\tau_i) = \pm \sqrt{\left| A^2 - [\sigma_{avg} \cdot (i \cdot \Delta\tau - c\tau_{max})]^2 \right|} + \theta_{shift} \quad (S1)$$

Equation (S1) shows that the potential is dependent on the $\Delta\tau$ value which depends on $\Delta\theta$, and consequently any changes in $\Delta\theta$ will directly be reflected in the sequence of simulated discrete potential

values. A smaller $\Delta\tau$ means the difference in potential between corresponding time steps is smaller and will provide a more refined current response, which will be reflected in the peak flux value as shown in Figure S1.

Figure S1 shows the peak flux plotted against the corresponding $\Delta\theta$ values where the blue dots represent results obtained from the triangular potential wave and the green diamond shapes represent results obtained from the semi-circular potential wave. The other two parameters, h and ω , were set to 10^{-6} and 1.1 respectively. With increasing $\Delta\theta$ the absolute peak flux value obtained from the semi-circular potential wave decreases indicating the system is not convergent. Meanwhile between $\Delta\theta = 10^{-4}$ and $\Delta\theta = 10^{-5}$ the peak flux does not change and thus shows our results with $\Delta\theta = 10^{-4}$ are convergent.

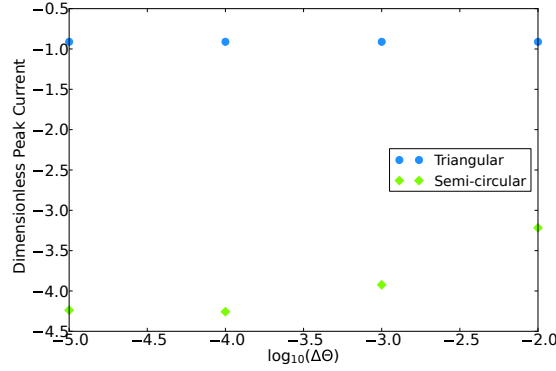


Figure S1: Peak flux of triangular and semi-circular results plotted against \log_{10} of the corresponding $\Delta\theta$ values with $\sigma = 3.89$ and $K_0 = 10^2$. The blue dots represent results obtained using the triangular potential wave and the green diamond shapes represent results obtained using the semi-circular potential wave.

We next run a convergence test for varying h values, which is the initial grid space of the expanding spatial grid². Figure S2 shows the peak flux plotted against \log_{10} of the h values using the same colors as Figure S1. Here, $\Delta\theta = 10^{-4}$ and $\omega = 1.1$. It is clear that the varying h 's do not affect the peak flux values for either the triangular or the semi-circular potential wave results and hence our choice of using $h = 10^{-6}$ is justified.

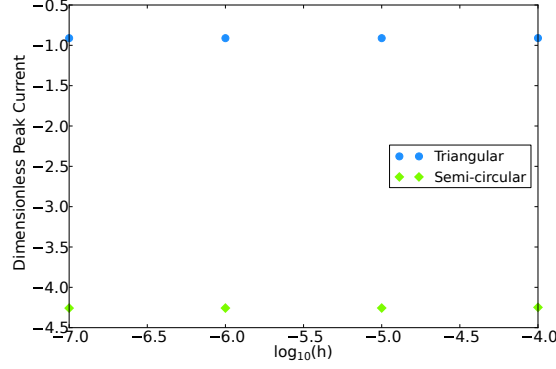


Figure S2: Peak flux of triangular and semi-circular results plotted against \log_{10} of corresponding h values with $\sigma = 3.89$ and $K_0 = 10^2$. The same color scheme as Figure S1 is used.

Lastly we show the convergence test results for varying ω values, which is the expanding factor of the expanding spatial grid². Figure S3 shows the peak flux plotted against the ω values using the same colors as Figure S1. $\Delta\theta = 10^{-4}$ and $h = 10^{-6}$. Similar to h values, varying ω 's in the range tested show no effect on the peak flux for both the triangular and semi-circular results, indicating our results using $\omega = 1.1$ are convergent.

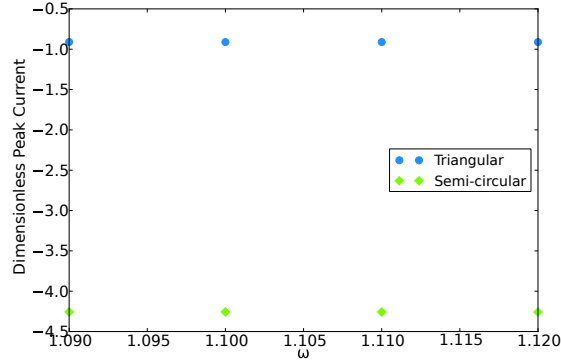


Figure S3: Peak flux of triangular and semi-circular results plotted against corresponding ω values with $\sigma = 3.89$ and $K_0 = 10^2$. The same color scheme as Figure S1 is used.

The three convergence tests show that our results reported in the paper are all convergent up to $K_0 = 10^2$, however, for higher K_0 's where the peak approaches infinity, full convergence is not necessarily achieved as, with increasing K_0 , the peak flux approaches an infinite value. In the next section we discuss the voltammetric features when a dimensionless scan rate of $\sigma_{avg} = 0.389$ and $\sigma_{avg} = 10^{-4}$ are applied to the semi-circular potential wave.

S2 Voltammetric response for different dimensionless scan rates

We first discuss the voltammograms obtained with a dimensionless scan rate of $\sigma_{avg} = 0.389$. Figure S4a and S4b show the voltammetric response for the triangular and semi-circular potential waves using various K_0 values with an arrow to indicate the direction of the sweep. The peak flux values from these two figures were used to plot the data in Figure 4 of the paper. Due to the relatively slow scan rate, the triangular results show a near steady-state response for lower K_0 's, and the reversible peak flux of the semi-circular results are not as pronounced as the results of $\sigma_{avg} = 3.89$.

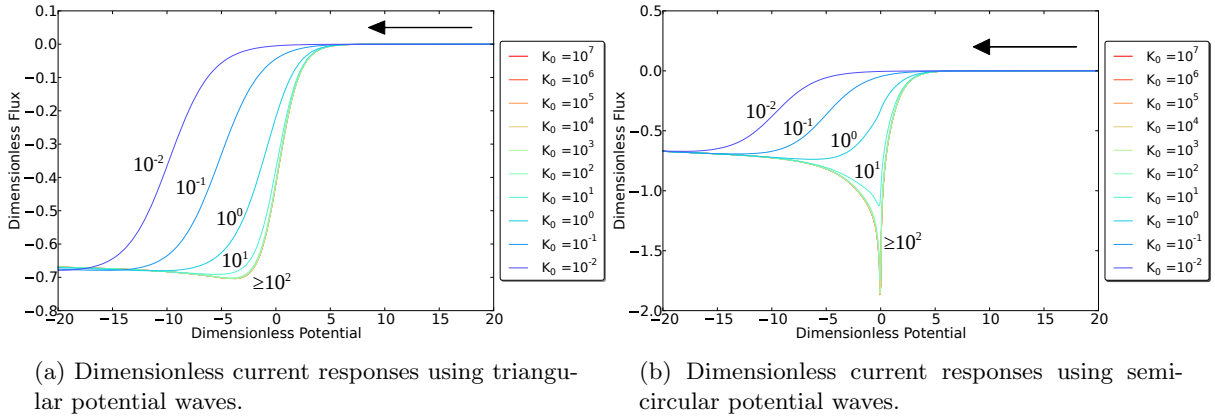


Figure S4: Dimensionless current responses using (a)triangular potential waves and (b)semi-circular potential waves with various K_0 values and $\sigma = 0.389$. Each voltammogram is color-coded and the corresponding K_0 values are listed in the label and the arrow indicates the direction of the sweep. The graphs approach the irreversible limit (low K_0) towards the left and reversible limit (high K_0) towards the right.

We second discuss the extreme case mentioned in the paper, one when the scan rate is relatively slow to give a full steady-state current response. Figure S5a and S5b show the voltammetric response when the scan rate is $\sigma_{avg} = 10^{-4}$ for the same K_0 's as reported in the paper. The pink dotted line shows the steady-state limiting current predicted by the following expression²:

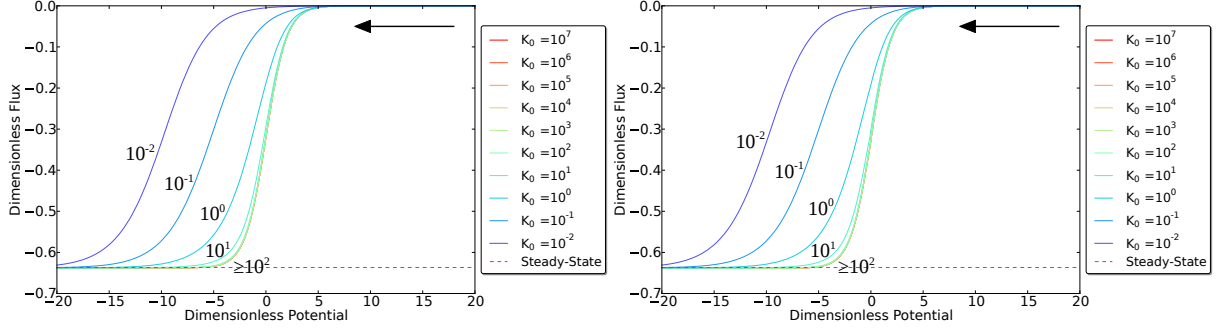
$$I_{lim,ss} = -4F\epsilon c_j^* D_j \quad (S2)$$

which in dimensionless terms is:

$$J_{lim,ss} = -\frac{2}{\pi} C_j^* d_j \quad (S3)$$

All triangular results converge to a steady value indicating the system is fully steady-state, and from simple observation it is clear that the two figures produce nearly identical curves for every K_0 value. One might expect to see a relatively sharp peak in the semi-circular results at the midpoint of the potential window for high K_0 values, however, this is not the case. The reason is that since the system is near the

steady-state and, at all times, the diffusion is fast compared to the reaction kinetics, changes in scan rate are less reflected in the current response.



(a) Dimensionless current response using triangular potential wave with various K_0 values. The pink dotted line represents the steady-state limiting flux predicted by Equation (S3). For more detail, refer to Figure S4a.

(b) Dimensionless current response using semi-circular potential wave with various K_0 values. The pink dotted line represents the steady-state limiting flux predicted by Equation (S3). For more detail, refer to Figure S4b.

Figure S5

We further compare the semi-circular concentration profile against that obtained using a triangular potential wave when the dimensionless potential is zero in order to check whether the two methods produce identical current responses. Figures S6a and S6b show the concentration profiles obtained from the triangular and semi-circular potential waves respectively at the timestep $\tau = 200000$. We chose this particular timestep because it is when $\theta(\tau) = 0$ for both waves and is where the transiently infinite scan rate is observed in the semi-circular potential wave. Hence any discrepancies between the two methods will be reflected maximally at this timestep.

Simple examination of the two figures give the impression that the two concentration profiles are equal across the entire space. We see a depletion of species at and near the electrode surface, represented via the light green and yellow with a radial diffusion near the edge at $R = 1$. Since we cannot determine the real difference between the two concentration profiles through observation, we additionally plot their percent differences.

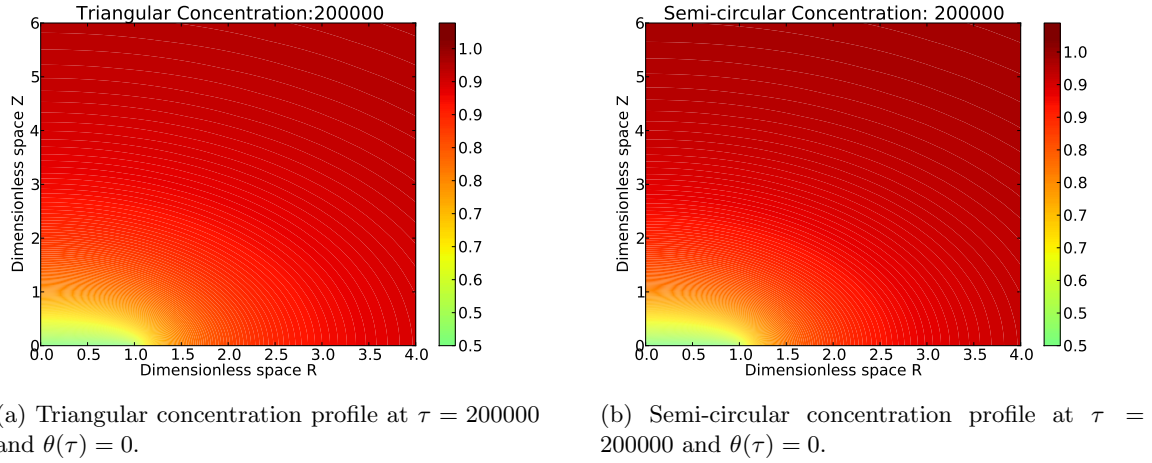


Figure S6

Figure S7a shows the percent difference between Figures S6a and S6b, and Figure S7b shows a zoomed up version of Figure S7a for clarity. From Figure S7b we see that there are some percent differences at and near the electrode surface between $R = 0$ and $R = 0.6$ but decreases further out, which we can see through the color changes. The biggest percent difference is observed at the edge of the electrode at $R = 1$, as can be seen with the bright colors. This is expected because this is where radial diffusion occurs and thus changes in the diffusion will be pronounced most significantly in this area.

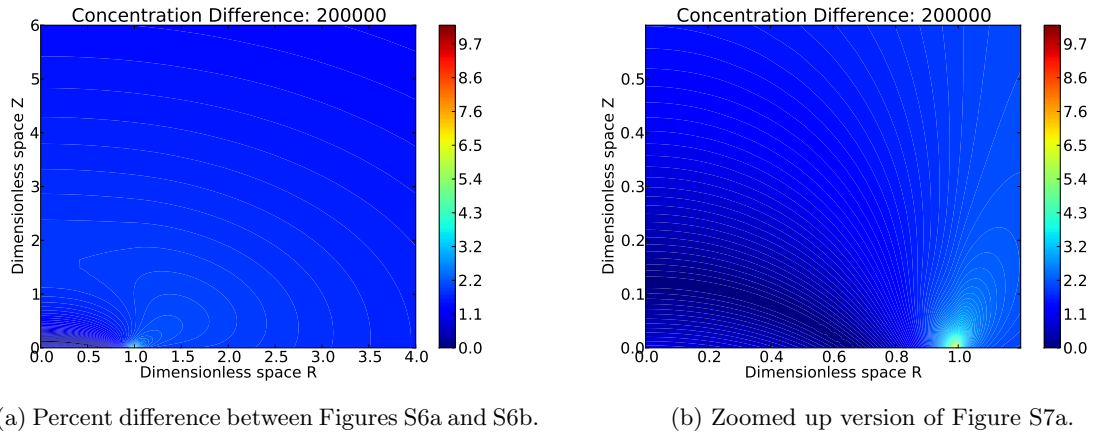


Figure S7

From our analysis of Figure S7b, we know that even though the concentration profiles obtained from the triangular and semi-circular potential wave methods are very similar, there are some percent differences, which reaches up to approximately 10% for the chosen set of numerical parameters. Nevertheless, the difference reflected in the current response is negligible and both methods achieve a full steady-state. Consequently the semi-circular method loses its advantage over the triangular method and hence cannot

be used for the determination of K_0 .

S3 Evaluating E_f^0 and K_0

The following section provides a numerical example of the proposed analysis. We first detail how the data used in the example is generated by numerical simulations, before we, second, conduct the analysis. Third, we compare the results of the analysis with the parameters used in the generation of the analyzed data.

S3.1 Generating experimental data

In this section, we provide a numerical example of the use of the curves in Figure 4 of the paper. To this end, we first assign E_f^0 , k_0 , and α on which basis we simulate data in dimensionless coordinates, which is converted back to dimensional coordinates. The analysis is then carried out as if E_f^0 and k_0 were unknown. $E_f^0 = -0.168V$, $k_0 = 3.2 \cdot 10^{-2}ms^{-1}$, and α and σ are set to 0.5 and 3.89 respectively since the analysis and results reported in the paper also consider $\alpha = 0.5$ and $\sigma = 3.89$. Figure S8 shows the supposed experimental dimensional peak currents plotted against their corresponding E_{centre} values.

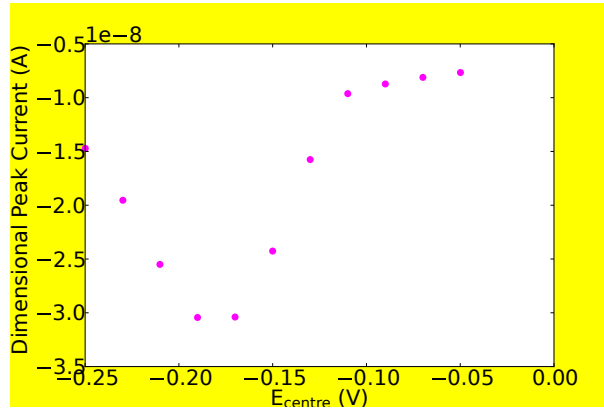


Figure S8: Dimensional peak currents plotted against their corresponding E_{centre} values. $\alpha = 0.5$ and $\nu = 1.0Vs^{-1}$.

S3.2 Determining E_f^0 and estimating K_0

From Figure S8, we can approximate the absolute maximum peak current and the corresponding E_{centre} value at which it occurs, which we denote as E_{max} . Using the transformation table given in the paper, we convert the maximum peak current to its dimensionless value (approximately -5.25) and compare it with the curves in Figure 4, which provides θ_{shift} for the theoretical maximum peak current (henceforth denoted as θ_{max}) and a rough estimate of K_0 . With E_{max} and θ_{max} available, we can

calculate E_f^0 through the equation:

$$\theta_{max} = \frac{F}{RT}(E_{max} - E_f^0) \quad (S4)$$

giving $E_f^0 = -0.168V$ in which $\theta_{max} = -0.45$ and $E_{max} = -0.18V$

S3.3 Determining K_0

Once the formal potential is determined, another LSV is performed using a potential window that is symmetric with respect to the formal potential, $E_{centre} = E_f^0$. The dimensional peak current is then converted to dimensionless coordinates. The dimensionless peak current when $E_{centre} = -0.168V$ is -4.95 , and we use this value to determine the K_0 based on Figure 3 of the paper. Assuming the green diamonds in Figure 3 produce a continuous curve, we can see that the dimensionless peak current is observed at approximately $2.5 = \log_{10}(K_0)$, which is equivalent to $K_0 = 3.16 \cdot 10^2$. Again using Table 1, K_0 can be converted to its dimensional form, $k_0 = 3.16 \cdot 10^{-2}ms^{-1}$.

S3.4 Accuracy of our method

The exact values used in the simulation of the analysed data are $E_f^0 = -0.168V$ and $k_0 = 3.2 \cdot 10^{-2}ms^{-1}$. The exact formal potential and that determined through the proposed method are in excellent agreement. The estimated k_0 differs by approximately 1.25%, which is also in good agreement.

Readers should note that the K_0 analysis is extremely sensitive to the peak current which itself is sensitive to θ_{shift} , and thus a slight difference in the estimated E_f^0 can result in significant changes in the K_0 value obtained. For example, if we underestimate θ_{max} and use a value of -0.4 for the calculation of E_f^0 we will obtain a value of $-0.17V$, which gives a dimensionless peak current of -5.01 . If we then use this value for the K_0 analysis, the result is $K_0 = 3.98 \cdot 10^2$ and gives a 24% error. Nonetheless, the method can still be used for a useful estimate of the rate constant even under such extreme conditions.

References

- [1] Y. Uchida, E. Kätelhön, R. G. Compton, Linear sweep voltammetry with non-triangular waveforms at a microdisc electrode, *Journal of Electroanalytical Chemistry* 823 (2018) 465 – 473.
- [2] R. G. Compton, E. Laborda, K. R. Ward, *Understanding Voltammetry: Simulation of Electrode Processes*, Imperial College Press, 2013.